

Research Progress on Environmental Compatibility Evaluation of Stainless Steels with Liquid Lead-Bismuth Eutectic for Lead-Cooled Fast Reactors

Authors: Tan Jibo, Zhang Xinrui, Xue Baoquan, Zhang Ziyu, Wu Xinqiang

Date: 2025-06-19T17:31:19+00:00

Abstract

The environmental compatibility of structural materials in liquid lead-bismuth is a bottleneck restricting the research, development, and construction of lead-cooled fast reactors. 9-12Cr ferritic-martensitic steels and austenitic stainless steels are preferred materials for key components in lead-cooled fast reactors, but they face severe liquid metal corrosion (oxidation and dissolution) issues in high-temperature liquid lead-bismuth environments; typically, appropriate amounts of Si or Al are added to the alloys to enhance their resistance to liquid lead-bismuth corrosion. This paper reviews the research progress on oxidation, dissolution, slow strain rate tensile testing, creep, fatigue, and crack propagation of 9-12Cr ferritic-martensitic steels, austenitic stainless steels, Si-enhanced ferritic-martensitic and austenitic steels, and Al-containing austenitic stainless steels in liquid lead-bismuth environments, discusses the liquid metal embrittlement susceptibility and damage mechanisms of ferritic-martensitic steels (body-centered cubic) and austenitic stainless steels (face-centered cubic) in liquid lead-bismuth environments, identifies existing problems in current research, and prospects future research directions.

Full Text

Preamble

Vol. XX, No. X, XXX 20XX NUCLEAR TECHNIQUES

Research on Environmental Compatibility Evaluation of Stainless Steels for Lead-Cooled Fast Reactors

Jibo Tan¹, Xinrui Zhang^{1,2}, Baoquan Xue¹, Ziyu Zhang¹, Xinqiang Wu^{1*}

¹CAS Key Laboratory of Nuclear Materials and Safety Assessment, Institute of Metal Research, Chinese Academy of Sciences, Shenyang 110016, China

²School of Materials Science and Engineering, Northeastern University, Shenyang 110819, China

Abstract

The environmental compatibility of structural materials in liquid lead-bismuth eutectic (LBE) represents a critical bottleneck restricting the development and construction of lead-cooled fast reactors. While 9–12Cr ferritic/martensitic steels and austenitic stainless steels are preferred candidate materials for key reactor components, they face severe liquid metal corrosion (oxidation and dissolution) challenges in high-temperature LBE environments. Alloying with appropriate amounts of Si or Al is commonly employed to enhance corrosion resistance. This paper reviews recent research progress on oxidation, dissolution, slow strain rate tensile behavior, creep, fatigue, and crack propagation of 9–12Cr ferritic/martensitic steels, austenitic stainless steels, Si-enhanced variants, and Al-containing austenitic stainless steels in LBE. The liquid metal embrittlement sensitivity and damage mechanisms of ferritic/martensitic steels (body-centered cubic) and austenitic stainless steels (face-centered cubic) in LBE are discussed, current research limitations are identified, and future research directions are proposed.

Keywords: Lead-cooled fast reactor, Stainless steel, Liquid metal corrosion, Liquid metal embrittlement, Mechanical property

China is actively and safely developing nuclear power in accordance with the “three-step” strategy of thermal reactors → fast reactors → fusion reactors. While commercial pressurized water reactors currently constitute the main reactor type, advanced reactor designs including lead-cooled fast reactors, sodium-cooled fast reactors, and thorium-based molten salt reactors are under active development. Lead-cooled fast reactors employ a closed fuel cycle that can utilize U-238 with a relative abundance of 99% (compared to less than 1% for U-235 used in pressurized water reactors), thereby supporting the sustainable development of nuclear fission energy. Pure lead or lead-bismuth eutectic alloys offer advantages such as low melting point, high boiling point, favorable neutron economy, and chemical inertness, making them preferred coolants for lead-cooled fast reactors [1–3]. Internationally, numerous lead-cooled fast reactor designs have been proposed, including Europe’s ELFR, Russia’s BREST-OD-300 and SVBR-100, America’s SSTAR, Korea’s URANUS-40, China’s CiADS and CLEAR-I, and Japan’s PBWFR, with their main parameters listed in [3].

Lead-cooled fast reactors typically have a design lifetime of 15–30 years. Key components such as fuel cladding and reactor vessels experience coupled damage from irradiation (150 dpa, displacements per atom), high temperature (300–650°C), complex stress states, and dynamic (2 m/s) LBE corrosion during long-term service. Their performance under these conditions critically affects re-

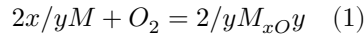
actor safety. Consequently, materials for key components must satisfy several requirements: (1) excellent comprehensive mechanical properties including high-temperature strength, ductility, creep resistance, fatigue resistance, and creep-fatigue performance; (2) good resistance to irradiation swelling to maintain dimensional stability; (3) good resistance to irradiation hardening and embrittlement; and (4) good resistance to environmental degradation in LBE, such as oxidation, dissolution, and liquid metal embrittlement [2,4].

9–12Cr ferritic/martensitic steels exhibit excellent high-temperature mechanical properties and irradiation damage resistance, with extensive service data accumulated from fossil power plants and substantial irradiation damage data as candidate first-wall materials for fusion reactors [5], making them preferred materials for key lead-cooled fast reactor components. Austenitic stainless steels offer good strength, ductility, and corrosion resistance, with extensive service data from pressurized water reactor nuclear power plants, also making them preferred materials for key components. Novel materials such as FeCrAl alloys, high-entropy alloys, and SiC, with their outstanding oxidation resistance, are candidate materials for key lead-cooled fast reactor components [2]. Adding appropriate amounts of Si or Al to ferritic/martensitic and austenitic stainless steels represents a primary approach to enhancing LBE corrosion resistance. In recent years, Si- or Al-enhanced stainless steels have become materials of choice for fuel cladding and heat exchangers in lead-cooled fast reactors, as exemplified by Russia's BREST-OD-300 currently under construction. Additionally, according to public reports, the China Institute of Atomic Energy has achieved industrial-scale production of Si-enhanced stainless steels resistant to LBE corrosion. Therefore, a systematic summary of research progress on the degradation behavior of 9–12Cr ferritic/martensitic steels, austenitic stainless steels, and their modified variants (Si-enhanced ferritic/martensitic and austenitic steels, Al-containing austenitic stainless steels) in LBE environments is warranted.

1. Thermodynamic Analysis of Corrosion

Material degradation in LBE primarily occurs through dissolution and oxidation. [Figure 1: see original paper] shows the solubility curves of various metallic elements in LBE, demonstrating that metallic elements exhibit relatively high solubility in high-temperature LBE, particularly Ni, Mn, and Cu [1]. Consequently, alloys with high Ni, Mn, or Cu content, such as nickel-based superalloys, are generally unsuitable for lead-cooled fast reactors. However, Ni, Mn, and Cu are typical austenite-stabilizing elements essential for single-phase face-centered cubic alloys like 316 stainless steel. To effectively mitigate dissolution corrosion, protective oxide films must form on the surface to prevent intimate contact between the substrate and LBE.

The oxidation of alloying elements in LBE, under standard atmospheric pressure, consumes 1 mol O_2 to form oxide MO according to reaction (1):



where M represents an alloying element. By consulting thermodynamic data [6], the Gibbs free energy change (ΔG° , kJ/mol) for M O formation can be calculated.

Oxide stability is thermodynamically dependent on temperature and oxygen partial pressure. The relationships between ΔG° , enthalpy change (ΔH° , kJ/mol), entropy change (ΔS° , J/mol · K), and temperature (T, K) for common oxides in LBE are listed in . The dissolved oxygen concentration in LBE follows Sievert's law, and the relationship between oxygen partial pressure (p_{O_2} , bar) and dissolved oxygen concentration (C_O , wt.%) is given by equation (2) [7]:

$$p_{O_2} = 10^{13.558 - \frac{20182}{T}} \cdot C_O^2 \quad (2)$$

The relationship between ΔG° and p_{O_2} is expressed by equations (3) and (4) [7]:

$$\Delta G = \Delta G^\circ + RT \ln(p_{O_2}) \quad (3)$$

$$\Delta G^\circ = -RT \ln K \quad (4)$$

where R is the gas constant (8.3145 J/mol · K). Based on these relationships, Gibbs free energy-temperature-dissolved oxygen concentration diagrams for element oxidation in LBE can be constructed, as shown in [Figure 2: see original paper], enabling assessment of oxide thermodynamic stability under various temperature and dissolved oxygen conditions. The oxygen affinity of elements in LBE follows the sequence: Al > Ti > Si > Cr > Fe > Ni > Pb, indicating that Al, Ti, Si, and Cr oxides exhibit high stability in high-temperature LBE. Therefore, Al, Ti, and Si are commonly added as corrosion-resistant elements to 9–12Cr ferritic/martensitic steels and austenitic stainless steels to improve LBE corrosion resistance. Notably, oxidation in LBE also depends on the activity of elements in the alloy, as expressed by equation (5) [8–10]:

$$a_M = \gamma_M \cdot X_M \quad (5)$$

where a_M is the activity of element M in the alloy (typically < 1). Consequently, the minimum dissolved oxygen concentration required for oxide formation in the alloy is usually higher than the predicted values shown in [Figure 2: see original paper].

2. 9–12Cr Ferritic/Martensitic Steels

2.1 Corrosion Behavior in LBE

9–12Cr ferritic/martensitic steels exhibit excellent resistance to neutron irradiation swelling and good high-temperature ($< 600^{\circ}\text{C}$) creep performance, making them preferred fuel cladding materials for lead-cooled fast reactors. Major grades include T91, P92, HT-9, E911, and Manet II [2,11–13], typically containing ≤ 0.5 wt.% Si. Numerous studies have investigated their environmental compatibility in LBE, revealing that at temperatures below 450°C , dense Fe_3O_4 and FeCr_2O_4 oxide films typically form on material surfaces, providing effective protection against severe oxidation and dissolution corrosion. At temperatures above 550°C , under high oxygen conditions, materials develop a porous outer Fe_3O_4 layer, a relatively dense inner FeCr_2O_4 layer, and a Cr-selective internal oxidation zone, while under low oxygen conditions, dissolution corrosion occurs [13–20].

[Figure 3: see original paper] shows typical cross-sectional morphologies of oxide films on T91 steel after 1000 h exposure in LBE at 550°C under different oxygen concentrations [13]. At dissolved oxygen concentrations above 1.26×10^{-6} wt.%, oxidation occurs, while below 1.41×10^{-8} wt.%, LBE penetration and dissolution corrosion take place. Additionally, high LBE flow velocity (~ 2 m/s) can cause oxide film spallation from ferritic/martensitic steel surfaces, bringing the substrate into direct contact with LBE and accelerating mass transfer, further degrading oxidation and dissolution resistance [15,16,19].

To improve LBE corrosion resistance of 9–12Cr ferritic/martensitic steels, 1–2 wt.% Si is typically added to promote formation of dense Si-rich oxide films that effectively protect the substrate. Typical chemical compositions of Si-enhanced ferritic/martensitic steels are listed in . Wang et al. [21] reported that Si content must exceed 0.5 wt.% in 9Cr ferritic/martensitic steel to effectively enhance LBE corrosion resistance. M.P. Short et al. [22] studied the corrosion behavior of Fe-2Cr-2Si in LBE at 600 – 715°C (506 h), finding that a Fe-Cr-Si-rich oxide film formed, particularly nanoscale Si-rich oxides in the inner layer, significantly improving corrosion resistance in both high- and low-oxygen LBE environments. Rong et al. [23,24] reported that after 10,000 h exposure in dynamic oxygen-controlled LBE at 550°C (0.3 m/s, 10^{-7} – 10^{-6} wt.%), 12Cr-Si steel formed Si-Cr-rich oxides at the oxide/substrate interface, reducing the oxidation rate by approximately half compared to HT-9 steel. Pre-oxidation in 1% oxygen atmosphere at 720°C for 1 h further improved corrosion resistance in LBE.

Polekhina et al. [25] investigated long-term corrosion behavior of EP-823-sh steel in dynamic oxygen-controlled LBE at 630°C (4 – 8×10^{-7} wt.%, ~ 2 m/s, 2500 h), observing non-uniform oxide films 0.25–18 μm thick composed primarily of Si-Mn-containing Fe-Cr spinel, with B-rich phases observable in the internal oxidation zone. This steel has been used as fuel cladding material for Russia's BREST-OD-300 lead-cooled fast reactor [26,27]. Russia has also developed high-Si (1.9 wt.%) EI-852 ferritic/martensitic steel, though it exhibits significant

irradiation embrittlement [27]. Yang et al. [28] developed SIMP steel, demonstrating superior irradiation resistance, high-temperature oxidation resistance, LBE corrosion resistance, and creep performance (at 550°C) compared to T91 steel. Lu et al. [29] also developed 9Cr-Si ferritic/martensitic steel, finding that Si addition effectively improved corrosion resistance in static oxygen-saturated LBE at 550°C.

However, Schroer et al. [30] studied the corrosion behavior of 1.4718 ferritic/martensitic steel in dynamic oxygen-controlled LBE at 450°C and 550°C (10^{-7} – 10^{-6} wt.%, 2 m/s, 1200–15,000 h), finding that while corrosion resistance significantly improved compared to T91 at 450°C, the effect was minimal at 550°C. At 550°C, the cross-sectional oxide structure consisted of a thin outer spinel oxide film and a deep Si-selective intergranular internal oxidation zone. Shi et al. [31] similarly observed that 9Cr ferritic/martensitic steels with Si additions (0.7, 1 wt.%) developed thinner outer spinel oxide films and deeper Si-oxidized internal zones after 2000 h exposure in oxygen-controlled LBE (10^{-6} wt.%) at 550°C and 600°C, suggesting that this structural change enhanced adhesion between substrate and oxide film, thereby improving corrosion resistance, as shown in [Figure 4: see original paper].

In summary, Si addition (1%) promotes formation of Si-rich oxide films on material surfaces, enhancing LBE corrosion resistance of 9–12Cr ferritic/martensitic steels, particularly for 12Cr grades.

Irradiation/LBE synergy significantly affects fuel cladding corrosion behavior. Yao et al. [32] studied in-situ Ar ion irradiation (1.36 dpa) coupled with dynamic LBE corrosion (350°C, saturated oxygen, 0.6 m/s, 92 h) of SIMP steel (11Cr, 1.43Si), finding that irradiation enhanced elemental diffusion and accelerated oxidation, increasing oxide film thickness from 110 nm (0 dpa) to 500 nm (1.36 dpa). Frazer et al. [33] investigated in-situ proton irradiation (~22 dpa) coupled with LBE corrosion (420°C, saturated oxygen, 80 h) of HT-9 ferritic/martensitic steel (12Cr, 0.4Si), also observing irradiation-accelerated oxidation with oxide thickness increasing from 1 μ m to 13 μ m. Demir et al. [34] recently studied Fe-12Cr-2Si alloy under in-situ proton irradiation in LBE (4 h), finding that at 675°C in low-oxygen LBE, the alloy formed Cr- and Si-rich oxides that effectively protected the substrate, with proton irradiation having minimal effect on corrosion behavior. However, current studies on structural material corrosion in simulated irradiation-LBE coupling environments have experimental durations <100 h and maximum irradiation doses of only 22 dpa, whereas lead-cooled fast reactor design lifetimes are typically 15–30 years with fuel cladding irradiation doses up to 150 dpa. Long-term irradiation-corrosion coupling data are essential for component lifetime design and operational safety assessment.

2.2 Mechanical Behavior in LBE

The mechanical performance of ferritic/martensitic steels in LBE critically affects component safety, encompassing slow strain rate tensile behavior, fatigue,

creep, and crack propagation. Numerous studies have evaluated the effects of temperature, dissolved oxygen concentration, strain rate, irradiation hardening, and Si content on liquid metal embrittlement sensitivity [35–44]. Results show that elongation-temperature curves typically exhibit a “ductility trough.” As shown in [Figure 5: see original paper] [40,41], minimum ductility and maximum embrittlement sensitivity occur at approximately 350°C, with fracture surfaces showing characteristic quasi-cleavage features. At low dissolved oxygen concentrations, protective oxide films cannot form, allowing direct LBE-substrate contact, dissolution corrosion, and quasi-cleavage fracture, significantly reducing ductility.

Strain rate also affects embrittlement sensitivity by influencing oxide film rupture/repair and LBE-substrate contact time. Under saturated oxygen conditions, higher strain rates increase embrittlement sensitivity, whereas under low-oxygen conditions, lower strain rates increase sensitivity. Irradiation effects on embrittlement correlate with hardening degree. When irradiation and tensile test temperatures are comparable (samples irradiated first, then tested in LBE), irradiation hardening during tensile testing enhances embrittlement sensitivity. When irradiation temperature exceeds test temperature, no hardening occurs and embrittlement sensitivity remains essentially unchanged [42].

Although Si addition improves LBE corrosion resistance, it promotes Laves phase precipitation, raising the ductile-to-brittle transition temperature [24]. First-principles calculations indicate that Si-induced reductions in surface energy and Young’s modulus significantly increase embrittlement sensitivity of BCC Fe in LBE [44]. However, systematic studies on slow strain rate tensile behavior of Si-enhanced ferritic/martensitic steels in LBE are lacking and needed to evaluate liquid metal embrittlement sensitivity.

Key factors affecting low-cycle fatigue performance of ferritic/martensitic steels in LBE include strain amplitude, temperature, dissolved oxygen concentration, and strain rate [45–51]. T91 steel fatigue life in LBE increases with decreasing strain amplitude, with environmental effects more pronounced at high strain amplitudes, as shown in [Figure 6a: see original paper] [45]. Fatigue life-temperature curves exhibit “valley and peak” characteristics. As shown in [Figure 6b: see original paper], T91 steel fatigue life increases with temperature in 150–250°C and 350–500°C ranges, but decreases with temperature in 250–350°C and 500–550°C ranges [46,47]. T91 steel fatigue life in oxygen-saturated LBE is typically higher than in oxygen-depleted conditions ([Figure 6a: see original paper]), though this has only been studied at 350°C; high-temperature (550°C) effects require further investigation. Strain rate effects are temperature-dependent: at 350°C, strain rate has minimal effect on T91 fatigue life ([Figure 6c: see original paper]) [45], but at 550°C in oxygen-saturated LBE, fatigue life decreases significantly with decreasing strain rate (0.004–0.4% s⁻¹) ([Figure 6d: see original paper]) [48]. Current studies on corrosion fatigue behavior of ferritic/martensitic steels focus on low temperatures (≤ 350°C); systematic investigation at typical service temperatures (550°C) is needed.

Fracture toughness, creep, and crack propagation properties of ferritic/martensitic steels are also significantly degraded in LBE. Studies show that creep rates of T91, P92, and HT-9 steels in LBE at 550–650°C may increase by up to 50 times compared to air [11,12,37,52]. FeCrAl coatings on T91 steel can improve creep resistance in LBE at 550°C [53]. Fracture toughness of T91 steel in LBE at 200–355°C decreases by up to ~30% compared to air, typically decreasing with decreasing tensile rate [54–58]. Fatigue crack propagation rates of T91 steel in LBE at 150–450°C increase significantly compared to air (saturated oxygen, load ratio 0.1, loading frequency 0.1 Hz), with LBE wetting crack tips, diffusing into the substrate, and causing quasi-cleavage fracture [59,60].

3. Austenitic Stainless Steels

3.1 Corrosion Behavior in LBE

Austenitic stainless steels, with their good fracture toughness, corrosion resistance, and medium-to-high temperature mechanical properties, are preferred materials for lead-cooled fast reactor components, with major grades including 316, 304, and 15-15Ti [2,24,61–63]. Studies show that in high-oxygen LBE, austenitic stainless steels develop oxide films consisting of a porous outer Fe_3O_4 layer and a dense inner FeCr_2O_4 layer [16,24,61–66]. Below 450°C, these oxide films effectively protect the substrate, but above 450°C, they become ineffective, with severe intergranular oxidation occurring under high-oxygen conditions and dissolution corrosion (particularly Ni-selective dissolution leading to ferritization) under low-oxygen conditions. [Figure 7: see original paper] shows typical cross-sectional oxide morphology on 316L stainless steel after 2000 h exposure in oxygen-saturated LBE at 550°C, exhibiting intergranular oxidation, especially at high-angle grain boundaries [62]. High LBE flow velocity (~2 m/s) can cause oxide spallation, promoting Ni dissolution and accelerating corrosion [66].

Si addition improves LBE corrosion resistance of austenitic stainless steels by forming dense Si-rich protective oxide films. Typical chemical compositions of Si-enhanced austenitic stainless steels are listed in . Schroer et al. [67] studied long-term corrosion (40,000 h) of 1.4571 stainless steel (1 wt.% Si) in dynamic oxygen-controlled LBE at 550°C (2 m/s, 10^{-9} – 10^{-5} and 10^{-6} wt.%). Samples exposed to low oxygen (10^{-9} – 10^{-5} wt.%) experienced severe dissolution, while those at 10^{-6} wt.% formed protective Cr-Si-rich oxide films in some regions with dissolution in others. Kurata et al. [68] studied 18Cr-20Ni-5Si steel in static LBE at 450°C and 550°C, finding continuous submicron Si-rich oxide films after 3000 h that effectively prevented dissolution corrosion. Roy et al. [69] investigated 18Cr-15Ni-3.7Si and 21Cr-11Ni-1.6Si steels in static LBE at 520°C (10^{-9} – 10^{-4} wt.% oxygen for first 30 h, then 10^{-4} wt.%), observing nanoscale oxide films with good corrosion resistance after 1850 h. Chen et al. [24,70–72] developed Fe-15Cr-9Ni-2Si stainless steel based on 316 stainless steel. After 3000 h in static oxygen-saturated LBE at 550°C, the oxide film consisted of porous outer Fe_3O_4 and dense inner Fe-Cr spinel, with nanoscale SiO_2 particles uniformly

distributed in the spinel and at oxide/substrate interface nanovoids ([Figure 8: see original paper]). Unlike severe intergranular oxidation in 316 stainless steel, Fe-15Cr-9Ni-2Si showed no significant intergranular oxidation, possibly due to enhanced oxide densification and impeded elemental diffusion by uniformly distributed nanoscale SiO₂ particles. Wu et al. [24] also reported that Si-enhanced austenitic stainless steels exhibited significantly reduced oxidation rates compared to 316H in static oxygen-saturated LBE at 550°C and showed no dissolution after 1500 h in dynamic oxygen-controlled LBE (0.3 m/s, 10⁻⁶–10⁻⁷ wt.%), attributed to Si enrichment in the inner oxide layer. However, Kurata et al. [73,74] reported that Si-enhanced (2.4–5.8 wt.%) austenitic stainless steels still experienced dissolution corrosion during long-term exposure in low-oxygen (10⁻⁸ wt.%) LBE at 550°C. In summary, appropriate Si addition improves oxidation and dissolution resistance of austenitic stainless steels in LBE and represents a primary direction for reactor vessel material development.

Al addition also improves LBE corrosion resistance of austenitic stainless steels. Al-containing austenitic stainless steels typically have compositions of Fe-(12–35)Ni-(12–20)Cr-(2–6)Al-(0.1–3)Nb. Zhang et al. [75,76] studied Fe-23Ni-15Cr-3Al steel in LBE at 600°C, observing dissolution corrosion at 10⁻⁸ wt.% oxygen, but formation of ~100 nm Cr-Al-rich oxide films (especially continuous Al₂O₃ at the oxide/substrate interface) at 10⁻⁶ wt.% oxygen that effectively prevented dissolution. Under oxygen-saturated conditions, ~5 μm oxide films formed with outer Fe₃O₄ + minor Cr-Al-rich oxides, middle Fe-Cr spinel, and inner Cr-rich oxide + minor Al-rich oxide, with localized dissolution in some regions. Cold-work-induced dislocations and grain boundaries promoted Cr and Al diffusion, facilitating rapid formation of protective oxide films. Shen et al. [77] studied Fe-14Ni-14Cr-2.5Al steel in dynamic oxygen-controlled LBE at 550°C (1.8 m/s, 5 × 10⁻⁷–5 × 10⁻⁶ wt.%), forming continuous nanoscale Al-rich oxide films with excellent corrosion resistance. Tsisar et al. [78] investigated long-term corrosion (10,000 h) of Fe-14Cr-2Mn-20Ni-0.5Cu-3Al and Fe-14Cr-5Mn-12Ni-3Cu-2.5Al steels in oxygen-controlled LBE at 500°C (10⁻⁹–10⁻⁶ wt.%), finding submicron Al-Cr-rich oxide films with good corrosion resistance, though the high-Ni steel experienced localized dissolution at low oxygen (10⁻⁹ wt.%). These results demonstrate that Al-containing austenitic stainless steels form Al-rich oxide films, particularly continuous Al₂O₃ at the oxide/substrate interface, providing good corrosion resistance but with localized dissolution risks under low-oxygen (<10⁻⁸ wt.%) conditions.

3.2 Mechanical Behavior in LBE

Research on austenitic stainless steel mechanical behavior in LBE has focused on slow strain rate tensile, creep, fatigue, and crack propagation properties. Sapundjiev et al. [79] studied slow strain rate tensile behavior of 316L stainless steel in LBE at 200°C (5 × 10⁻⁶ s⁻¹), finding no embrittlement in either unirradiated or irradiated (1.5 dpa) conditions. Bosch et al. [80] and Stergar et al. [81] similarly reported no embrittlement in irradiated (1.5 dpa) 316L stain-

less steel during slow strain rate tests in LBE at 200, 350, and 450°C. Petersson et al. [82] investigated Al-containing austenitic stainless steels in low-oxygen (10^{-10} wt.%) LBE during slow strain rate tests (140–600°C, $5 \times 10^{-5} \text{ s}^{-1}$), observing no embrittlement below 550°C but intergranular cracking above 570°C. Serre et al. [83] also reported reduced elongation and liquid metal embrittlement in Al-containing austenitic stainless steels in liquid lead above 500°C. Gong et al. [84] studied creep behavior of 15-15Ti stainless steel in LBE at 550°C and 600°C (10^{-10} wt.%-oxygen-saturated), finding significantly increased creep rates compared to air due to dissolution corrosion and intergranular cracking.

Yas'kiv et al. [85] studied low-cycle fatigue behavior of Fe–18Cr–10Ni in liquid lead at 350°C, observing significant fatigue life reduction with increasing strain amplitude. Ding et al. [86] investigated low-cycle fatigue of 316LN stainless steel tubular specimens (filled internally with LBE) in LBE at 400°C, finding fatigue life slightly reduced compared to air only at high strain amplitudes ($\approx 0.8 \text{ } \sigma_{400^\circ\text{C}}$); systematic studies at typical service temperatures (400–500°C) are needed.

4. Liquid Metal Embrittlement Mechanism

Liquid metal embrittlement causes significant degradation of structural material properties including ductility, fracture toughness, creep, and fatigue, posing a major threat to safe operation of lead-cooled fast reactors. Body-centered cubic metals exhibit high embrittlement sensitivity, while face-centered cubic metals show lower sensitivity. The primary characteristics of liquid metal embrittlement in LBE are reduced plasticity and quasi-cleavage fracture morphology. [Figure 11: see original paper] shows typical quasi-cleavage fracture features on T91 steel after low-cycle fatigue (bar specimens) and fatigue crack propagation (CT specimens) tests in LBE at 350°C [46,59].

Various embrittlement models have been proposed for solid metal/liquid metal systems, including adsorption-induced surface energy reduction, adsorption-induced atomic bond weakening, adsorption-promoted dislocation emission, adsorption-enhanced work hardening, and stress-assisted dissolution [2]. T91 steel exhibits severe embrittlement in specific LBE environments, with macroscopic transgranular quasi-cleavage fracture and microscopic cracking along deformation-induced grain boundaries and high-density dislocation interfaces. No single model adequately explains T91 embrittlement mechanisms.

Gong et al. [45,51] proposed a new interpretation based on adsorption-induced atomic bond weakening, suggesting that Pb-Bi adsorption weakens atomic bonds at crack tips while dislocation pile-up causes hardening. When the critical stress for dislocation motion exceeds the weakened bond strength due to Pb-Bi adsorption, atomic bond rupture leads to cleavage fracture. Xue et al. [46,59] proposed that fatigue brittle cracks in T91 steel in LBE at 150–450°C appear transgranular macroscopically but propagate preferentially along $1\text{--}5^\circ$ subgrain boundaries formed by local plastic deformation at

crack tips. Atomic-scale characterization ([Figure 12: see original paper]) revealed that LBE wets the plastic deformation zone at crack tips, with Pb-Bi atom segregation, short-range ordered Pb/Bi-Fe superstructures, and Pb-Bi clusters/precipitates/films observed on deformation subgrain boundaries [59]. Intergranular Pb-Bi atoms reduce atomic bonding strength, forming microcracks along subgrain boundaries and initiating brittle fracture. These results reveal the liquid metal embrittlement mechanism of quasi-cleavage fracture in T91 steel at the atomic scale. Additionally, at 550°C in oxygen-saturated LBE, T91 steel undergoes dynamic recrystallization at fatigue crack tips, with severe intergranular oxidation and Pb-Bi penetration reducing grain boundary cohesion, leading to oxidation + Pb-Bi penetration-dominated embrittlement [48].

Although slow strain rate tensile and low-cycle fatigue tests of 316L(N) stainless steel in LBE show typical ductile fracture features and low embrittlement sensitivity, Xue et al. [90] reported increased fatigue crack propagation rates and quasi-cleavage fracture features in 316LN stainless steel in oxygen-saturated LBE at 300°C and 400°C, indicating liquid metal embrittlement. The primary cause may be crevice effects within cracks during fatigue crack propagation, reducing dissolved oxygen concentration at crack tips [91], while plastic deformation zones ahead of crack tips facilitate direct LBE wetting of the substrate and accelerate penetration under stress assistance [92,93], increasing embrittlement sensitivity. [Figure 13: see original paper] shows microstructural features at a fatigue crack tip in 316LN stainless steel at 400°C in oxygen-saturated LBE [90], with Pb-Bi atoms preferentially diffusing along deformation twin boundaries and dislocation interfaces accompanied by Ni-selective dissolution. Pb_7Bi_3 particles, Pb-Bi segregation, microvoids, and interface cracking were observed at deformation twin boundaries and high-density dislocation interfaces ahead of crack tips, reducing cohesion and causing brittle crack propagation along microstructural interfaces. Serre et al. [83] also observed reduced elongation and intergranular cracking in Al-containing austenitic stainless steel in high-temperature liquid lead (500°C), indicating liquid metal embrittlement. Luo et al. [94] observed Bi atoms forming bilayer or trilayer structures at Ni grain boundaries, where liquid Bi separates grains and Bi-Bi bonds are much weaker than Ni-Ni bonds, causing Ni embrittlement. Yu et al. [95] observed segregation-induced ordered superstructures at general grain boundaries in Ni-Bi systems that can embrittle polycrystalline engineering alloys. Duscher et al. [96] studied liquid metal embrittlement in Cu/Bi systems, finding that segregated Bi atoms embrittle by inducing Zn-like electronic structures in surrounding Cu atoms. Thus, although face-centered cubic alloys have lower embrittlement sensitivity, Pb-Bi can still penetrate and segregate along grain boundaries, deformation twin boundaries, and high-density dislocation interfaces, causing quasi-cleavage or intergranular fracture.

5. Summary and Outlook

1. 9–12Cr ferritic/martensitic steels and 316 stainless steel are preferred materials for fuel cladding and reactor vessels in lead-cooled fast reactors. However, Fe_3O_4 and FeCr_2O_4 oxide films formed in high-temperature ($>450^\circ\text{C}$) LBE cannot effectively protect the substrate, leading to severe oxidation corrosion with intergranular oxidation under high-oxygen conditions and dissolution corrosion under low-oxygen conditions, with further performance degradation at high flow velocities (~ 2 m/s).
2. Adding appropriate Si or Al to 9–12Cr ferritic/martensitic and austenitic stainless steels promotes formation of Si-rich oxide films that effectively improve LBE corrosion resistance. Current developments include Si-enhanced ferritic/martensitic steels (1–2 wt.% Si), Si-enhanced austenitic stainless steels (2.5–5 wt.% Si), and Al-containing austenitic stainless steels (2–6 wt.% Al). However, dissolution corrosion risks remain in high-temperature, low-oxygen ($<10^{-8}$ wt.%) LBE.
3. 9–12Cr ferritic/martensitic steels exhibit high embrittlement sensitivity in LBE, typically undergoing quasi-cleavage fracture ($\sim 450^\circ\text{C}$) or intergranular fracture ($\sim 550^\circ\text{C}$) under loading, reducing ductility, fracture toughness, fatigue, creep, and crack propagation properties. The quasi-cleavage embrittlement mechanism involves LBE wetting of the plastic deformation zone at crack tips, forming Pb-Bi segregation, short-range ordered Pb/Bi-Fe superstructures, and Pb-Bi clusters/precipitates/films on deformation subgrain boundaries that reduce atomic bonding strength. High-temperature intergranular fracture results from intergranular oxidation combined with LBE penetration along grain boundaries.
4. 316L(N) stainless steel shows low embrittlement sensitivity in LBE, typically exhibiting ductile fracture under loading with ductility, fracture toughness, and fatigue properties comparable to or slightly lower than in air. However, quasi-cleavage fracture occurs during fatigue crack propagation, with the embrittlement mechanism involving Pb-Bi penetration and segregation along grain boundaries, deformation twin boundaries, and high-density dislocation interfaces.
5. Current embrittlement mechanism interpretations are based primarily on post-test microstructural analysis. Future work should include in-situ TEM loading tests after LBE wetting, combined with molecular dynamics and first-principles calculations to analyze interactions between Pb-Bi atoms and defects (vacancies, dislocations, grain boundaries) under loading, fundamentally revealing liquid metal embrittlement mechanisms.
6. Limited research exists on creep, fatigue, and creep-fatigue behavior of ferritic/martensitic and austenitic stainless steels at typical service temperatures (500–550°C) in LBE. Intergranular oxidation occurs at high temperatures, and corrosion-stress interactions may degrade service per-

formance, requiring systematic investigation.

7. Si and Al are ferrite-stabilizing elements that typically reduce fracture toughness, increase ductile-to-brittle transition temperature, and worsen irradiation embrittlement resistance when added to ferritic/martensitic and austenitic stainless steels. While corrosion behavior of Si-enhanced and Al-containing steels in LBE has been studied, systematic investigation of their service behavior and damage mechanisms under simulated irradiation-thermal-mechanical-corrosion coupling conditions is needed to support engineering applications in lead-cooled fast reactors.

Author Contributions: Jibo Tan conceived the overall idea and wrote the manuscript; Xinrui Zhang contributed the corrosion section; Baoquan Xue contributed the embrittlement mechanism section; Ziyu Zhang reviewed and revised the manuscript; Xinqiang Wu coordinated the entire work and performed final review and revision.

References

- [1] Handbook on Lead-Bismuth Eutectic Alloy and Lead Properties, Materials Compatibility, Thermal-hydraulics and Technologies [B], 2015, OECD/NEA No.6195. DOI: 10.1787/42dcd531-en
- [2] X. Gong, M. P. Short, T. Auger, E. Charalampopoulou, K Lambrinou. Environmental degradation of structural materials in liquid lead-and lead-bismuth eutectic-cooled reactors [J]. Prog. Mater. Sci. 126 (2022) 100920. DOI:10.1016/j.pmatsci.2022.100920
- [3] Handbook of Generation IV Nuclear Reactors [B]. Chapter 6, Lead-cooled fast reactor, 2016, P119-155. DOI: 10.1115/1.4035327
- [4] G.S. Was. Challenges to the use of ion irradiation for emulating reactor irradiation[J]. J. Mater. Res. 30(2015) 1158-1182. DOI: 10.1557/jmr.2015.73
- [5] Qunying Huang, Chunjing Li, Yanfen Li, Shaojun Liu, Yican Wu, Jiangang Li, Farong Wan, Xin Ju, Yiyin Shan, Jinnan Yu, Shengyun Zhu, Pinyuan Zhang, Jianfeng Yang, Fusheng Han, Fusheng Han, Mingguang Kong, Heqin Li, Takeo Muroga, Takuya Nagasaka. Research progress on China low activation martensitic steel CLAM[J]. Nuclear Science and Engineering, 1(2007)41-49. DOI:10.3321/j.issn:0258-0918.2007.01.009
- [6] W. M. Haynes. CRC Handbook of Chemistry and Physics [M]. Florida, 2016. DOI: 10.1021/ja2071225
- [7] C.F.E. Schroer, J. Konys. Physical Chemistry of Corrosion and Oxygen Control in Liquid Lead and Lead-Bismuth Eutectic, in, 2007. DOI: 10.5445/IR/270069895
- [8] C.H. Xu, W. Gao, Y.D. He. High temperature oxidation behaviour of FeAl intermetallics-oxide scales formed in ambient atmosphere[J]. Scr. Mater. 42 (2000) 975–980. DOI:10.1016/S1359-6462(00)00327-4

- [9] J. Eldridge, K.L. Komarek. Thermodynamic properties of solid iron-aluminum alloys[J]. *Trans. Metall. Soc. AIME* 230 (1964) 226. DOI: 10.1021/j100783a012
- [10] W. Wang, Z.G. Zhu, L.J. Yang, J.T. Lu, J.Y. Huang, J.B. Tan, W.J. Kuang. Superior corrosion resistance of a slurry FeAl coating on 316LN stainless steel in 550 °C liquid lead-bismuth eutectic[J]. *Corros. Sci.*, 227(2024) 111757. DOI:10.1016/j.corsci.2023.111757
- [11] M. Yurechko, C. Schroer, A. Skrypnik. Creep-to-rupture of the steel P92 at 650°C in oxygen-controlled stagnant LBE in comparison to air[J]. *J. Nucl. Mater.*, 432(1-3) (2013) 90-97. DOI:10.1016/j.jnucmat.2012.07.029
- [12] J. Xiao, Z. Zhong, T. Wen, X. Yu, H. Wang, K. Zhao, C. Liu, H. Zhuo, S. Qiu, G. Liu, Y. Li, X. Gong. Synergy of stress and corrosion in a 12Cr ferritic/martensitic steel exposed to static liquid lead-bismuth eutectic at 550 °C[J]. *Corros. Sci.* 222 (2023) 111404. DOI:10.1016/j.corsci.2023.111404
- [13] Z. G. Zhu, Q. Zhang, J.B. Tan, X.Q. Wu, H.B. Ma, Z.Y. Zhang, Q.S. Ren, E.-H. Han, X. Wang. Corrosion behavior of T91 steel in liquid lead-bismuth eutectic at 550 °C: Effects of exposure time and dissolved oxygen concentration[J]. *Corros. Sci.* 204 (2022) 110405. DOI: 10.1016/j.corsci.2022.110405
- [14] D. Sapundjiev, S. Van Dyck, W. Bogaerts. Liquid metal corrosion of T91 and A316L materials in Pb-Bi eutectic at temperatures 400-600°C[J]. *Corros. Sci.* 48 (2006): 577-94. DOI: 10.1016/j.corsci.2005.04.001
- [15] C. Schroer, Z. Voß, O. Wedemeyer, J. Novotny, J. Konys. Oxidation of steel T91 in flowing lead-bismuth eutectic (LBE) at 550°C[J]. *J. Nucl. Mater.*, 356 (2006) 189-197. DOI: 10.1016/j.jnucmat.2006.05.009
- [16] S.J. Tian. Growth and exfoliation behaviour of the oxide scale on 316L and T91 in flowing liquid lead-bismuth eutectic at 480°C[J]. *Oxid. Met.* 93(2020):183-194. DOI: 10.1007/s11085-019-09953-7
- [17] L. Luo, Z. Xiao, M. Zhang, Z. Jiang, J. Liu, W. Huang, L. Sun. Honeycomb structure with oxygen-poor pores at the top of magnetite layer on a martensitic steel CLAM exposed to lead-bismuth eutectic at 500 °C[J]. *Corros. Sci.* 204 (2022) 110410. DOI: 10.1016/j.corsci.2022.110410
- [18] V. Tsisar, S. Gavrilov, C. Schroer, E. Stergar. Long-term corrosion performance of T91 ferritic/martensitic steel at 400°C in flowing Pb-Bi eutectic with 2×10^{-7} mass% dissolved oxygen[J]. *Corros Sci* 2020;174:108852. DOI: 10.1016/j.corsci.2020.108852
- [19] V. Tsisar, C. Schroer, O. Wedemeyer, A. Skrypnik, J. Konys. Corrosion interaction of 9% Cr ferritic/martensitic steels at 450 and 550°C with flowing Pb-Bi eutectic containing 10^{-7} mass% dissolved oxygen[J]. *J Nucl Eng Radiat Sci* 5 (2019)031201. DOI: 10.1115/1.4041432
- [20] C. Schroer, V. Tsisar, A. Durand, O. Wedemeyer, A. Skrypnik, J. Konys.

Corrosion in iron and steel t91 caused by flowing lead-bismuth eutectic at 400°C and 10^{-7} mass% dissolved oxygen[J]. *J Nucl Eng Radiat Sci* (2019) 011006. DOI: 10.1115/1.4040937

[21] J. Wang, S.P. Lu, L.J. Rong, D.Z. Li, Y.Y. Li. Effect of silicon on the oxidation resistance of 9 wt.% Cr heat resistant steels in lead-bismuth eutectic at 550°C[J]. *Corros. Sci.* 102 (2016) 13-25. DOI:10.1016/j.corsci.2016.04.020

[22] M.P. Short, R.G. Ballinger, H.E. Hanninen. Corrosion resistance of alloys F91 and Fe-12Cr-2Si in lead-bismuth eutectic up to 715°C[J]. *J. Nucl. Mater.* 432 (2013) 71-79. DOI:10.1016/j.jnucmat.2012.11.010

[23] Xia Pan, Yangpeng Zhang, Zhihong Dong, Shenghu Chen, Haichang Jiang, Lijian Rong. Effect of pre-oxidation treatment on Pb-Bi corrosion resistance of 12Cr ferritic/martensitic steel[J]. *Acta Metallurgica Sinica*, 2024, 60(5): 639-649. DOI: 10.11900/0412.1961.2022.00267

[24] Xinqiang Wu, Lijian Rong, Jibo Tan, Shenghu Chen, Xiaofeng Hu, Yangpeng Zhang, Ziyu Zhang. Research progress on Pb-Bi corrosion resistant Si-enhanced ferritic/martensitic steels and austenitic stainless steels[J]. *Acta Metallurgica Sinica*, 2023, 59(4): 502-512. DOI: 10.11900/0412.1961.2022.00531

[25] N.A. Polekhina, I.Yu. Litovchenko, K.V. Almaeva, S.A. Akkuzin, V.V. Linnik, E.N. Moskvichev, V.M. Chernov, I.A. Naumenko, M.S. Saifutdinova, M.V. Leontieva-Smirnova. Special features of the surface layer structure of ferritic-martensitic EP-823-Sh steel after prolonged exposure to the flowing lead at 630°C under low oxygen concentration[J]. *J. Nucl. Mater.* 572 (2022) 154039. DOI:10.1016/j.jnucmat.2022.154039

[26] R. Isayev, N. Pukhareva, E. Malinovskiy, E. Korenevski, P. Dzhumaeva. Corrosion of EP823 Steel Cladding Under Heavy Liquid-Metal-Coolant Reactor Conditions: A Review[J]. *Nucl. Sci. Eng.*, (2024)1-19. DOI:10.1080/00295639.2024.2383110

[27] A.M. Dvoriashin, S.I. Porollo, Yu.V. Konobeev, N.I. Budylnkin, E.G. Mironova, A.G. Ioltukhovskiy, M.V. Leontyeva-Smirnova, F.A. Garner. Mechanical and microstructure properties of three Russian ferritic/martensitic steels irradiated in BN-350 reactor to 50 dpa at 490°C[J]. *J. Nucl. Mater.* 367-370 (2007) 92-96. DOI:10.1016/j.jnucmat.2007.03.161

[28] Ke Yang, Wei Yan, Zhiguang Wang, Yiyin Shan, Jinqiang Shi, Xianbo Shi, Wei Wang. Research progress on SIMP steel: A novel structural material for nuclear applications with high temperature resistance, irradiation tolerance and liquid metal corrosion resistance[J]. *Acta Metallurgica Sinica*, 2016, 52(10): 1207-1221. DOI:10.11900/0412.1961.2016.00320

[29] Yanhong Lu, Yuanyuan Song, Shenghu Chen, Lijian Rong. Effects of Al and Si on mechanical properties and Pb-Bi corrosion resistance of 9Cr2WVTa steel[J]. *Acta Metallurgica Sinica*, 2016, 52(3): 298-306. DOI: 10.11900/0412.1961.2015.00348

- [30] C. Schroer, V. Koch, O. Wedemeyer, A. Skrypnik, J. Konys. Silicon-containing ferritic/martensitic steel after exposure to oxygen-containing flowing lead–bismuth eutectic at 450 and 550°C[J]. *J. Nucl. Mater.* 469 (2016) 162-176. DOI:10.1016/j.jnucmat.2015.11.058
- [31] H. Shi, H. Wang, R. Fetzner, A. Heinzl, A. Weisenburger, K. Wang, A. Jianu, G. Müller. Influence of Si addition on the corrosion behavior of 9 wt% Cr ferritic/martensitic steels exposed to oxygen-controlled molten Pb-Bi eutectic at 550°C[J]. *Corros. Sci.* 193 (2021) 109871. DOI:10.1016/j.corsci.2021.109871
- [32] C. Yao, H. Zhang, H. Chang. Structure of surface oxides on martensitic steel under simultaneous ion irradiation and molten lead corrosion[J]. *Corros. Sci.*, (2022) DOI:10.1016/j.corsci.2021.109953
- [33] S. Frazer, S. Qvist, S. Parker. Degradation of HT9 under simultaneous ion beam irradiation and liquid metal corrosion[J]. *J. Nucl. Mater.*, 479(2016) 382-390. DOI:10.1016/j.jnucmat.2016.06.039
- [34] E. Demir, S. Ayyapan, W. Zhou, W. Cairang, K. B. Woller, M. P. Short, D. Kaoumi. Behavior of Fe-based alloys in a liquid lead-bismuth environment under simultaneous proton irradiation and corrosion[J]. *Acta Mater.* 284 (2025) 120578. DOI:10.1016/j.actamat.2024.120578
- [35] D.G. Kolman. A review of recent advances in the understanding of liquid metal embrittlement[J]. *Corrosion* 75 (2019) 42-57. DOI:10.5006/2904
- [36] X. Gong, E. Stergar, P. Marmy, S. Gavrilov. Tensile fracture behavior of notched 9Cr-1Mo ferritic-martensitic steel specimens in contact with liquid lead-bismuth eutectic at 350 °C[J]. *Mater. Sci. Eng. A* 692 (2017) 139-145. DOI:10.1016/j.msea.2017.03.067
- [37] H. Wang, X. Gong, J. Xiao, L. Chai, Z. Yu, H. Chen, K. Zhao, J. Zhou, G. Liu, Y. Chen, S. Qiu. Liquid metal embrittlement of 12Cr ferritic/martensitic steel thin-walled tubes exposed to liquid lead-bismuth eutectic[J]. *Corros. Sci.* 195 (2022) 110024. DOI:10.1016/j.corsci.2021.110024
- [38] Y. Dai, B. Long, X. Jia, H. Glasbrenner, K. Samec, F. Groeschel. Tensile tests and TEM investigations on LiSoR-2 to -4[J]. *J. Nucl. Mater.* 356 (2006) 256-263. DOI:10.1016/j.jnucmat.2006.05.010
- [39] F. Di Gabriele, A. Doubková, A. Hojná. Investigation of the sensitivity to EAC of steel T91 in contact with liquid LBE[J]. *J. Nucl. Mater.* 376 (2008) 307-311. DOI:10.1016/j.jnucmat.2008.02.029
- [40] B. Long, Z. Tong, F. Gröschel, Y. Dai. Liquid Pb–Bi embrittlement effects on the T91 steel after different heat treatments[J]. *J. Nucl. Mater.* 377 (2008) 219-224. DOI:10.1016/j.jnucmat.2008.02.050
- [41] J. Liu, W. Yan, W. Sha, W. Wang, Y. Shan, K. Yang. Effects of temperature and strain rate on the tensile behaviors of SIMP steel

in static lead bismuth eutectic[J]. *J. Nucl. Mater.* 473 (2016) 189-196. DOI:10.1016/j.jnucmat.2016.02.032

[42] B. Long, Y. Dai, N. Baluc. Investigation of liquid LBE embrittlement effects on irradiated ferritic/martensitic steels by slow-strain-rate tensile tests[J]. *J. Nucl. Mater.* 425 (2012) 236-242. DOI:10.1016/j.jnucmat.2011.11.036

[43] Z. Hamouche-Hadjem, T. Auger, I. Guillot, D. Gorse. Susceptibility to LME of 316L and T91 steels by LBE: Effect of strain rate[J]. *J. Nucl. Mater.* 376 (2008) 317-321. DOI:10.1016/j.jnucmat.2008.02.031

[44] X. Gong, L. Sun, F.F. Zhang, Y. Yin, X. Huang, H. Gong, Y. Liu. Effect of alloying elements on liquid metal embrittlement of pure BCC Fe in contact with liquid lead-bismuth eutectic: Experiments and first principles calculation[J]. *Corros. Sci.* 208 (2022) 110522. DOI:10.1016/j.corsci.2022.110522

[45] X. Gong, P. Marmy, B. Verlinden, M. Wevers, M. Seefeldt. Low cycle fatigue behavior of a modified 9Cr–1Mo ferritic–martensitic steel in lead–bismuth eutectic at 350 °C – Effects of oxygen concentration in the liquid metal and strain rate[J]. *Corros. Sci.* 94 (2015) 377–391. DOI:10.1016/j.corsci.2015.02.022

[46] B. Xue, W. Wang, J. Tan, W. Kuang, X. Wu, Z. Zhang, X. Wang, W. Ke. Insights into the fatigue damage mechanism of T91 steel in liquid lead-bismuth eutectic at 150–550 °C[J]. *Corros. Sci.* 232 (2024) 112007. DOI:10.1016/j.corsci.2024.112007

[47] B. Xue, J. Tan, Z. Zhang, X. Wang, X. Wu, E.-H. Han, W. Ke. Effect of temperature on low cycle fatigue behavior of T91 steel in liquid lead-bismuth eutectic environment at 150–550 °C[J]. *Int. J. Fatigue* 167 (2023) 107344. DOI:10.1016/j.ijfatigue.2022.107344

[48] B. Xue, J. Tan, X. Wu, Z. Zhang, X. Wang, W. Ke. Strain-rate dependent fatigue behavior of T91 steel at 550 °C of liquid lead-bismuth eutectic[J]. *Corros. Sci.* 240 (2024) 112433. DOI:10.1016/j.corsci.2024.112433

[49] X. Gong, P. Marmy, L. Qin, B. Verlinden, M. Wevers, M. Seefeldt. Temperature dependence of liquid metal embrittlement susceptibility of a modified 9Cr–1Mo steel under low cycle fatigue in lead–bismuth eutectic at 160–450 °C[J]. *J. Nucl. Mater.* 468 (2016) 289-298. DOI:10.1016/j.jnucmat.2015.06.021

[50] X. Gong, P. Marmy, Y. Yin. The role of oxide films in preventing liquid metal embrittlement of T91 steel exposed to liquid lead-bismuth eutectic[J]. *J. Nucl. Mater.* 509 (2018) 297-305. DOI:10.1016/j.jnucmat.2018.07.018

[51] X. Gong, P. Marmy, A. Volodin, B. Amin-Ahmadi, L. Qin, D. Schryvers, S. Gavrilov, E. Stergar, B. Verlinden, M. Wevers, M. Seefeldt. Multiscale investigation of quasi-brittle fracture characteristics in a 9Cr–1Mo ferritic–martensitic steel embrittled by liquid lead–bismuth under low cycle fatigue[J]. *Corros. Sci.* 102 (2016) 137-152. DOI:10.1016/j.corsci.2015.10.003

[52] A. Jianu, G. Müller, A. Weisenburger, A. Heinzl, C. Fazio, V.G.

Markov, A.D. Kashtanov. Creep-to-rupture tests of T91 steel in flowing Pb–Bi eutectic melt at 550°C[J]. *J. Nucl. Mater.* 394 (2009) 102-108. DOI:10.1016/j.jnucmat.2009.08.013

[53] A. Weisenburger, A. Jianu, W. An, R. Fetzner, M.D. Giacco, A. Heinzl, G. Müller, V.G. Markov, A.D. Kashtanov. Creep, creep-rupture tests of Al-surface-alloyed T91 steel in liquid lead bismuth at 500 and 550°C[J]. *J. Nucl. Mater.* 431 (2012) 77-84. DOI:10.1016/j.jnucmat.2011.11.027

[54] J. Van den Bosch, G. Coen, A. Almazouzi, J. Degrieck. Fracture toughness assessment of ferritic–martensitic steel in liquid lead–bismuth eutectic[J]. *J. Nucl. Mater.* 385 (2009) 311-314. DOI:10.1016/j.jnucmat.2008.11.024

[55] T. Auger, D. Gorse, Z. Hamouche-Hadjem, J. Van den Bosch, G. Coen, A. Almazouzi, A. Hojna, K. Dalikova, F. Di Gabriele, M. Serrano, A. Gessi, P. Agostini, J.B. Vogt, I. Serre. Fracture mechanics behavior of the T91 martensitic steel in contact with liquid lead–bismuth eutectic for application in an accelerator driven system[J]. *J. Nucl. Mater.* 415 (2011) 293-301. DOI:10.1016/j.jnucmat.2011.04.021

[56] M.L. Martin, T. Auger, D.D. Johnson, I.M. Robertson. Liquid–metal-induced fracture mode of martensitic T91 steels[J]. *J. Nucl. Mater.* 426 (2012) 71-77. DOI:10.1016/j.jnucmat.2012.03.040

[57] B. Long, Y. Dai. Investigation of LBE embrittlement effects on the fracture properties of T91[J]. *J. Nucl. Mater.* 376 (2008) 341-345. DOI:10.1016/j.jnucmat.2008.02.022

[58] G. Coen, J. Van den Bosch, A. Almazouzi, J. Degrieck. Investigation of the effect of lead-bismuth eutectic on fracture properties of 316L[J]. *J. Nucl. Mater.* 396 (2010) 170-175. DOI:10.1016/j.jnucmat.2009.10.021

[59] B. Xue, J. Tan, X. Wu, Z. Zhang, W. Kuang, Q. Jin, X. Wang, E.-H. Han, W. Ke. Insights into fatigue crack propagation mechanism of T91 steel in liquid lead-bismuth eutectic at 150-450 °C[J]. *Corros. Sci.* 236 (2024) 112264. DOI:10.1016/j.corsci.2024.112264

[60] B. Xue, J. Tan, X. Wu, Z. Zhang, X. Wang. A novel monitoring system for fatigue crack length of compact specimen in liquid lead-bismuth eutectic[J]. *Nucl. Eng. Technol.* 56 (2023) 1887-1894. DOI:10.1016/j.net.2023.12.051

[61] C. Li, Y. Liu, F. Zhang. Erosion-corrosion of 304N austenitic steels in liquid PbBi flow perpendicular to steel surface[J]. *Mat. Charact.*, 175 (2021) 111054. DOI:10.1016/j.matchar.2021.111054

[62] C. Lu, M. Wang, J. Tan, X. Hao, T. Liang, Y. Ma. The initial enrichment behavior of nickel during the oxidation of 15–15Ti at 550 °C in liquid lead-bismuth eutectic: A new Ni-rich structure at grain boundary[J]. *Corros. Sci.* 244 (2025) 112664. DOI:10.1016/j.corsci.2024.112664

[63] S. Guo, J. Chen, Z. Ma, Q. Du, C. Lu, S. Xie, B. Long, D. Yun, L. Gu. The

roles of Ni segregation on the oxidation kinetics of austenitic stainless steel 316L exposed to oxygen-containing liquid lead-bismuth eutectic (LBE) [J]. *Corros. Sci.* 244 (2025) 112644. DOI:10.1016/j.corsci.2024.112644

[64] O. Klok, K. Lambrinou, S. Gavrilov, E. Stergar, J. Lim, T. Van der Donck. Effect of deformation twinning on dissolution corrosion of 316L stainless steels in contact with static liquid lead-bismuth eutectic (LBE) at 500°C[J]. *J. Nucl. Mater.* 510 (2018):556-567. DOI:10.1016/j.jnucmat.2018.08.030

[65] Y. Kurata, M. Futakawa, S. Saito. Comparison of the corrosion behaviour of austenitic and ferritic/martensitic steels exposed to static liquid Pb-Bi at 450 and 550°C[J]. *J. Nucl. Mater.* 343(2005):333-340. DOI: 10.1016/j.jnucmat.2004.07.064

[66] V. Tsisar, C. Schroer, O. Wedemeyer, A. Skrypnik, J. Konys. Effect of structural state and surface finishing on corrosion behaviour of 1.4970 austenitic steel at 400 and 500°C in flowing Pb-Bi eutectic with dissolved oxygen[J]. *J. Nucl. Eng. Rad. Sci.* 4 (2018) 041001. DOI:10.1115/1.4040422

[67] Carsten Schroer, Olaf Wedemeyer, Josef Novotny, Aleksandr Skrypnik, Jürgen Konys. Long-term service of austenitic steel 1.4571 as a container material for flowing lead-bismuth eutectic[J]. *J. Nucl. Mater.* 418 (2011) 8-15. DOI:10.1016/j.jnucmat.2011.07.026

[68] Y. Kurata, M. Futakawa. Excellent corrosion resistance of 18Cr-20Ni-5Si steel in liquid Pb-Bi[J]. *J. Nucl. Mater.* 325 (2004) 217-222. DOI:10.1016/j.jnucmat.2003.12.009

[69] Marion Roy, Laure Martinelli, Kevin Ginestar, Jerome Favregeon, Gerard Moulin. Dissolution and oxidation behaviour of various austenitic steels and Ni-rich alloys in lead-bismuth eutectic at 520°C[J]. *J. Nucl. Mater.* 468 (2016) 153-163. DOI:10.1016/j.jnucmat.2015.11.005

[70] A. Xie, S. Chen, L. Yin, N. He, C. Chen, L. Rong. Microstructural evolution of the inner oxide layer of a Si-modified austenitic stainless steel exposed to oxygen-saturated lead-bismuth eutectic (LBE): Toward the origin of LBE penetration[J]. *Corros. Sci.* 237 (2024) 112350. DOI:10.1016/j.corsci.2024.112350

[71] Yang Wu, Ang Xie, Shenghu Chen, Haichang Jiang, Lijian Rong. Liquid Pb-Bi eutectic corrosion behavior of NbC in Nb-containing austenitic stainless steel and its effect on oxide layer formation[J]. *Acta Metallurgica Sinica*, 61(2) (2025) 287-296. DOI: 10.11900/0412.1961.2022.00650

[72] A. Xie, S. Chen, S. Chen, H. Jiang, L. Rong. Austenite decomposition behavior adjacent to δ -ferrite in a Si-modified Fe-Cr-Ni austenitic stainless steel during thermal aging at 550°C[J]. *Acta Mater.* 272 (2024) 119948. DOI:10.1016/j.actamat.2024.119948

[73] Y. Kurata. Results of corrosion tests in liquid Pb-Bi at JAEA-temperature and oxygen concentration dependence, and corrosion properties of Si-enriched steels, in: OECD/NEA, 2010.

- [74] Y. Kurata. Corrosion behavior of Si-enriched steels for nuclear applications in liquid lead–bismuth[J]. *J. Nucl. Mater.* 437 (2013) 401-408. DOI:10.1016/j.jnucmat.2013.02.022
- [75] D. Zhang, X. Zhang, Y. Guo, J. Zhang, H. Ren, X. Zeng, Q. Yan. High-resolution characterization revealing the effect of dissolved oxygen in lead-bismuth eutectic (LBE) on oxide scale and subsurface phase transformation layer of alumina-forming austenitic (AFA) steel[J]. *Corros. Sci.* 245 (2025) 112671. DOI:10.1016/j.corsci.2024.112671
- [76] D. Zhang, X. Zhang, X. Zeng, J. Zhang, H. Ren, F. Meng, Q. Yan. High-resolution characterization of cold working effects on the oxidation behavior of alumina-forming austenitic (AFA) steel in lead-bismuth eutectic (LBE) with 10^{-6} wt.% oxygen at 600°C[J]. *Journal of Nuclear Materials* 607 (2025) 155691. DOI:10.1016/j.jnucmat.2025.155691
- [77] L. Shen, G. Cao, D. Lang, H. Peng, Y. Wen. Fe-14Ni-14Cr-2.5Al steel showing excellent corrosion-resistance in flowing LBE at 550 °C and high temperature strength[J]. *J. Nucl. Mater.* 587 (2023) 154703. DOI:10.1016/j.jnucmat.2023.154703
- [78] V. Tsisar, E. Stergar, S. Gavrilov, W. V. Renterghem, P. Louette, S. Lucas. Effect of variation in oxygen concentration in static Pb–Bi eutectic on long-term corrosion performance of Al-alloyed austenitic steels at 500 °C[J]. *Corros. Sci.* 195 (2022) 109963. DOI:10.1016/j.corsci.2021.109963
- [79] D. Sapundjiev, A. Al Mazouzi, S. Van Dyck. A study of the neutron irradiation effects on the susceptibility to embrittlement of A316L and T91 steels in lead–bismuth eutectic[J]. *J. Nucl. Mater.* 356 (2006) 229-236. DOI:10.1016/j.jnucmat.2006.05.030
- [80] J. Van den Bosch, G. Coen, R.W. Bosch, A. Almazouzi. TWIN ASTIR: First tensile results of T91 and 316L steel after neutron irradiation in contact with liquid lead–bismuth eutectic[J]. *J. Nucl. Mater.* 398 (2010) 68-72. DOI:10.1016/j.jnucmat.2009.10.012
- [81] E. Stergar, S.G. Eremin, S. Gavrilov, M. Lambrecht, O. Makarov, V. Iakovlev. Influence of LBE long term exposure and simultaneous fast neutron irradiation on the mechanical properties of T91 and 316L[J]. *J. Nucl. Mater.* 473 (2016) 28-34. DOI:10.1016/j.jnucmat.2016.02.008
- [82] C. Petersson, P. Szakálos, R. Pettersson. Influence of liquid lead and lead-bismuth eutectic on three alumina forming austenitic (AFA) steels through slow strain rate testing[J]. *J. Nucl. Mater.*, 603(2025) 155415. DOI:10.1016/j.jnucmat.2024.155415
- [83] S.I. Priol, J. B. Vogt. Mechanical behavior in liquid lead of Al_2O_3 coated 15-15Ti steel and an alumina-forming austenitic steel designed to mitigate their corrosion[J]. *Eng. Fail. Anal.*, 2022, 139: 106443. DOI:10.1016/j.engfailanal.2022.106443

- [84] X. Gong, Z. Yang, Y. Deng, J. Xiao, H. Wang, Z. Yu, Y. Yin. Creep failure of a solution-annealed 15-15Ti steel exposed to stagnant lead-bismuth eutectic at 550 and 600 °C[J]. *Mater. Sci. Eng. A* 798 (2020) 140230. DOI:10.1016/j.msea.2020.140230
- [85] O. I. Yas'kiv, V. M. Fedirko, I. S. Kukhar. Effect of Lead and Lead–Bismuth Eutectic Melts on the Fatigue Life of Steels of the Martensitic and Austenitic Classes[J]. *Mater. Sci.* 50(1)(2014)102–108. DOI:10.1007/s11003-014-9697-4
- [86] J. Ding, J. Tan, Z. Zhang. Low cycle fatigue behavior of 316LN stainless steel hollow specimen in air and liquid lead–bismuth eutectic[J]. *Int. J. Fatigue* 175(2023)107812. DOI:10.1016/j.ijfatigue.2023.107812
- [87] D. Kalkhof, M. Grosse. Influence of PbBi environment on the low-cycle fatigue behavior of SNS target container materials[J]. *J. Nucl. Mater.*, 318(2003) 143–150. DOI:10.1016/S0022-3115(03)00015-1
- [88] P. Marmy, X. Gong. LIMETS 3, a novel system for high strain fatigue testing in lead–bismuth eutectic[J]. *J. Nucl. Mater.*, 450(1–3)(2014)256–261. DOI:10.1016/j.jnucmat.2013.10.064
- [89] M. Chocholousek, E. Stergar, X. Gong, P. Marmy, S. Gavrillov, F. Ersoy. Mechanical/microstructural characteristics of environmentally-assisted degradation effects of steels in lead alloys and assessment of environmental degradation effects on performance of structural and functional components of MYRRHA ADS & LFR. *MatISSE – D5.42*, 2017.
- [90] B. Xue, J. Tan, X. Wu, Z. Zhang, W. Ke. Unveiling liquid Pb-Bi embrittlement of 316LN stainless steel under fatigue crack propagation tests through multiscale advanced characterization[J]. *Corros. Sci.* 246 (2025) 112752. DOI:10.1016/j.corsci.2025.112752
- [91] Y. Huang, F. Meng, J. Shi, L. Zhang, R. Yuan, Y. Chen, F. Zhang. Crevice corrosion behavior of 316L austenitic steel in static liquid lead-bismuth eutectic at 550°C[J]. *J. Nucl. Mater.*, 603(2025)155441. DOI:10.1016/j.jnucmat.2024.155441
- [92] W. Ludwig, E. Pereiro-López, D. Bellet. In situ investigation of liquid Ga penetration in Al bicrystal grain boundaries: grain boundary wetting or liquid metal embrittlement?[J]. *Acta Mater.* 53 (2005) 151-162. DOI:10.1016/j.actamat.2004.09.012
- [93] H. S. Nam, D. J. Srolovitz. Molecular dynamics simulation of Ga penetration along grain boundaries in Al: a dislocation climb mechanism[J]. *Phys. Rev. Lett.* 99, (2007) 025501. DOI:10.1103/PhysRevLett.99.025501
- [94] J. Luo, H. Cheng, K.M. Asl. The role of a bilayer interfacial phase on liquid metal embrittlement[J]. *Science*, 333(2011)1730-1733. DOI:10.1126/science.1208774
- [95] Z. Yu, Q. Gao, D. Yin, Y. Zhang, N. Zhou, S. Gregory, M. Widom,

J. Luo, M. P. Harmer. Segregation-induced ordered superstructures at general grain boundaries in a nickel-bismuth alloy[J]. Science 358(2017) 97-101. DOI:10.1126/science.aam8256

[96] G. Duscher, M.F. Chisholm, U. Alber, M. Ruhle. Bismuth-induced embrittlement of copper grain boundaries[J]. Nat Mater, 3(2004)621-626. DOI:10.1038/nmat1191

Note: Figure translations are in progress. See original paper for figures.

Source: ChinaXiv — Machine translation. Verify with original.